

# The Utilization of Pearson's Method to Analyze Piezoresistive Effect in Self-Sensing Cement Composite with Graphite

João Batista Lamari Palma e Silva<sup>a\*</sup> , Rosa Cristina Cecche Lintz<sup>a</sup> , Luísa Andréia Gache<sup>a</sup> 

<sup>a</sup>Universidade Estadual de Campinas, Faculdade de Tecnologia, Programa de Pós-Graduação em Tecnologia, Limeira, SP, Brasil.

Received: February 01, 2022; Revised: April 17, 2022; Accepted: June 12, 2022

Structural health monitoring (SHM) techniques aim to detect and prevent failures in constructions, although their use may require many sensors, which makes this technique expensive and laborious. In this sense, the use of self-sensing cementitious composites based on the piezoresistivity effect could be a solution to some monitoring problems. Thus, the evaluation of the piezoresistive effect is commonly performed by analyzing the linearity between mechanical forces and the variation of electrical resistivity, through the coefficient of determination ( $R^2$ ). However, this work has been used to perform the analysis through Pearson's correlation in samples of self-sensing cementitious composites with graphite addition. The results obtained have shown that Pearson's correlation has the potential to be used for the evaluation of the correlation between electrical resistivity and mechanical forces to verify the piezoresistive effect in the cases studied.

**Keywords:** *Self-sensing composite, piezoresistivity, cement, graphite, Pearson's correlation.*

## 1. Introduction

Structural health monitoring (SHM) techniques can provide increasing service life and construction safety, from early detection of strain, failures and damages<sup>1,2</sup>. However, continuous and wide-ranging monitoring may require high-cost investments due to the need for numerous sensors throughout the structure. So, using materials to be able to self-monitoring can be a solution to some problems with the use of sensors<sup>1,3</sup>. These materials can be created from a variety of matrices, such as polymers, asphalts, and cements<sup>4-9</sup>. The built-in sensors can make heterogeneity in the structure, which may cause some damage to the structure. While self-sensing composites make homogeneity to the structure<sup>2</sup>.

For the monitoring without using coupled or embedded sensors, the concrete structures need self-sensing cementitious composites in their manufacture to be able to detect changes in mechanical stress. Several electrical effects are the object of study for the application of self-sensing in materials, such as piezoresistivity. The piezoresistive effect allows the detection of mechanical strain and stress changes, as a result of the monitored electrical resistance change<sup>10,11</sup>. Further on the piezoresistivity, piezoelectric effect, capacitance and impedance are also used in self-sensing materials and sensor's manufacture and mechanism<sup>12-16</sup>. Also used in sensors and sensing platforms are nanomaterials, which are another large field of research that is growing<sup>17-20</sup>.

Regular concrete and mortar exhibit a few piezoresistive responses when under loads, that is not enough to consider as self-sensing materials<sup>21</sup>. At least up to a certain point, piezoresistive composites offer a certain electrical conductivity for concretes and mortars. This conductivity cannot be

too low to be considered the composite almost insulating, or too high to offer almost no electrical resistivity, as this would impede the measurement of the piezoresistive effect<sup>11</sup>. In other words, for the composite to be able to self-monitoring, a minimum conductive filler needs to be used, but not without prejudice to the highest possible electrical conductivity. This limit is called the "percolation threshold" as shown in Figure 1<sup>23</sup>.

As shown in Figure 2, as the self-sensing composite is compressed, the electrical resistivity decreases, as well as it is tensioned, it increases. In other words, this effect is what characterizes piezoresistivity, as a relationship between mechanical forces and the change in resistivity of the material. This change happens because conductive fillers move closer together or further apart, with compression or tension, thus altering the conductive paths. The change occurs linearly in the elastic regime of the composite, that is, up to a certain point in this relationship, as shown in Figure 3<sup>11</sup>, and the reversible strain happens in the elastic regime. As cracks appear after the elastic regime, the continuous paths are interrupted and the resistivity increases again<sup>2</sup>.

However, challenges must be overcome so that it is possible to use self-sensing composite to monitoring real structures, for example, to mitigate and reduce the influence of external environmental issues, which affect the performance of self-sensing<sup>26</sup>. In this way, it could be useful to use Pearson's correlation analysis ( $r$ ) to see how the piezoresistivity effect works in a cementitious composite.

Pearson's correlation analysis ( $r$ ) makes it possible to quantify the degree of association between two linear variables in a sample. This association has been described as a level of assessment of intensity and direction between the two compared variables. The correlation is great when the

\*e-mail: [lamaripalma@hotmail.com](mailto:lamaripalma@hotmail.com)

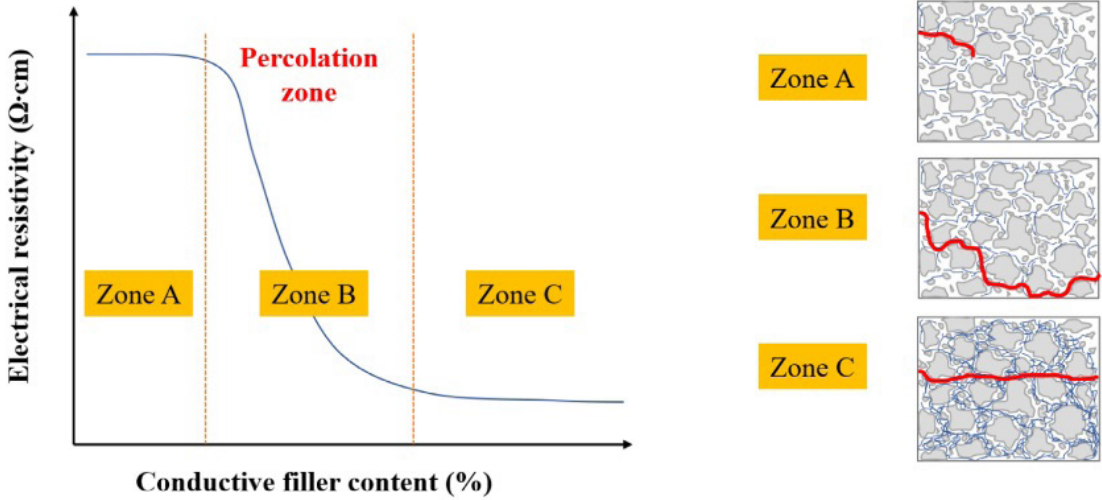


Figure 1. Schematic description of percolation theory. In Zone A, there is no conductive network. In Zone B, the resistivity is reduced abruptly, with few additions of fillers. Lastly, in Zone C, there is no significance in the reduction of resistivity when more fillers are added<sup>22</sup>.

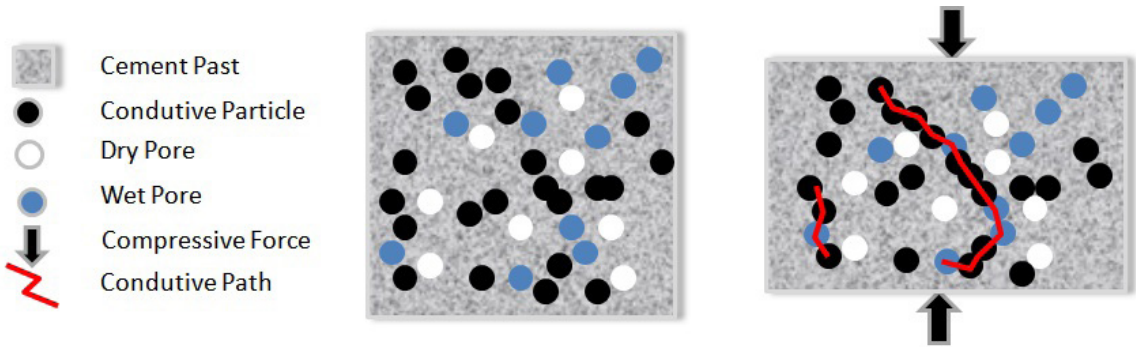


Figure 2. Conductive microstructure scheme in self-sensing cementitious (based on<sup>24</sup>).

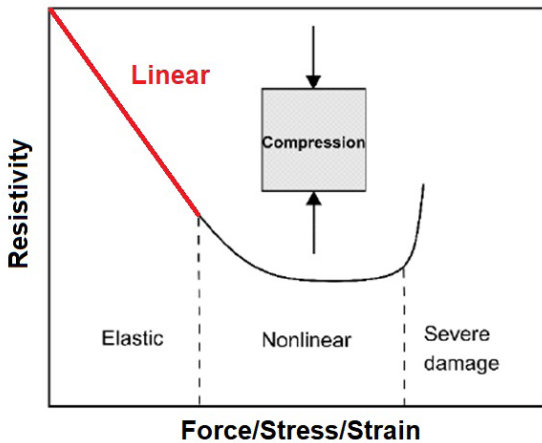


Figure 3. Graphic relationship between electrical resistivity and mechanical effort in a self-sensing composite (adapted from<sup>25</sup>).

coefficient is 1 (one) or -1 (negative one) and unsatisfactory when it approaches zero. This method of correlation, which today has the name of its author, was developed in 1985,

by Karl Pearson, and is obtained by Equation 1, where “x” and “y” are the variables, “ $\bar{x}$ ” and “ $\bar{y}$ ” the means, and “n” the number of variable pairs<sup>27</sup>.

$$r = \frac{\sum_{i=1}^n (x_i - \bar{x})(y_i - \bar{y})}{\sqrt{\sum_{i=1}^n (x_i - \bar{x})^2} \sqrt{\sum_{i=1}^n (y_i - \bar{y})^2}} \tag{1}$$

There are some limitations to Pearson’s method, such as the need for analyzed data to have a bivariate normal distribution and a linear relationship between them. Although the samples analyzed are significantly large in relation to the population, no more than two decimal places of the coefficient should be considered if the sample size <500, not even more than one decimal place, if the value of the coefficient is very small. For three decimal places, should be considered more than 100,000 the sample size<sup>28,29</sup>.

Researchers from different areas of science usually give names to the levels of Pearson’s coefficient intervals used to rank their results, such as “moderate correlation” between 0.6 and 0.7. However, like the classification for this range,

it is also called otherwise by other researchers who consider it strong and not moderate. That is to say, the interpretation of the coefficients varies substantially between the different areas of scientific research, and thus the use of classification nomenclature should be avoided, given the lack of absolute rules for interpreting the correlation between the variables<sup>30</sup>.

Even though researchers<sup>21,22,31-41</sup> have been working to analyze self-sensing behavior in cement composites, they have used only the coefficient of determination ( $R^2$ ) or graphic comparisons. However, this work does not aim to evaluate the mechanical properties of the cementitious composite but to use the Pearson's correlation to analyze the piezoresistive effect of self-sensing cement, which is why only graphite was used in the composite. Carbon-based materials have good electrical conductivity, so they are the materials most commonly used nowadays to make self-sensing cement composites<sup>42</sup>. Graphite is used, in a wide range of composites and materials, including smart structures, electromagnetic shielding, building, electric power, road engineering, aircraft parts, and thermal management<sup>8,42-44</sup>. Graphite powder was chosen because it is a low-cost material when compared with nanomaterials.

## 2. Materials and Methods

### 2.1. Materials

Following the literature<sup>45-47</sup> four mortar specimens were prepared for the piezoresistive test, in cubic shape samples with a 40 mm edge, dimensions recommended in NBR 16868-2<sup>48</sup> for compression test. The mortar mix rate was made in the following proportions of cement, sand, and graphite: T1C=1:4:0; T2C=1:4:0.125; T3C=1:4:0.250; and

T4C=1:4:0.375, in proportions to the cement mass, and these graphite proportions are within the range (0-0.4) used by<sup>49</sup>.

The water/cement ratio (w/c) of 0.50 used in the T1C mix could not be maintained in the other mixes, in which the following w/c ratios were used: T2C=0.75; T3C=1.05; and T4C=1.40, to get the consistency for molding the samples.

The specifications of the materials, according to the manufacturers, are: Portland cement, marketed by the company Votorantim Cimentos – Classification CP-II-F-32, 75% - 89% by mass of clinker + gypsum; 11% - 25% carbonate material; The quartz sand has a Fineness Modulus 2,03 according to NBR 7211<sup>50</sup>. The powdered graphite, marketed by Wonder - Carbon (Loss to Fire) >72%; Ash a maximum of 28%; maximum moisture 0.5%. In the Figure 4, the granulometric of sand and graphite are shown.

During the molding of the sample's specimens, 4 electrodes (aluminum plates) with a size of 35 x 20 x 0.1 mm were inserted, spaced 10 mm between each other and with 25 mm embedded in the mortar, as shown in Figure 5.

Although graphite improves the electrical conductivity of the cementitious composite, it generally causes a reduction in the composite's compressive strength. Much research reports the use of graphite with other fillers, such as polymer fibers or carbon, to improve the mechanical strength<sup>46,49,51</sup>.

### 2.2. Methods

The samples were tested by compression in a manual press, for three repetitions of each sample<sup>45,52</sup>, with a maximum load of nearly 2 kN<sup>31,32</sup>, since this load would not cause rupture of the samples, because it is a non-destructive test. The voltage (U) changes and force (compression) applied were recorded synchronously at a sampling rate of 10 Hz, using the scheme in Figure 6, which had a data acquisition

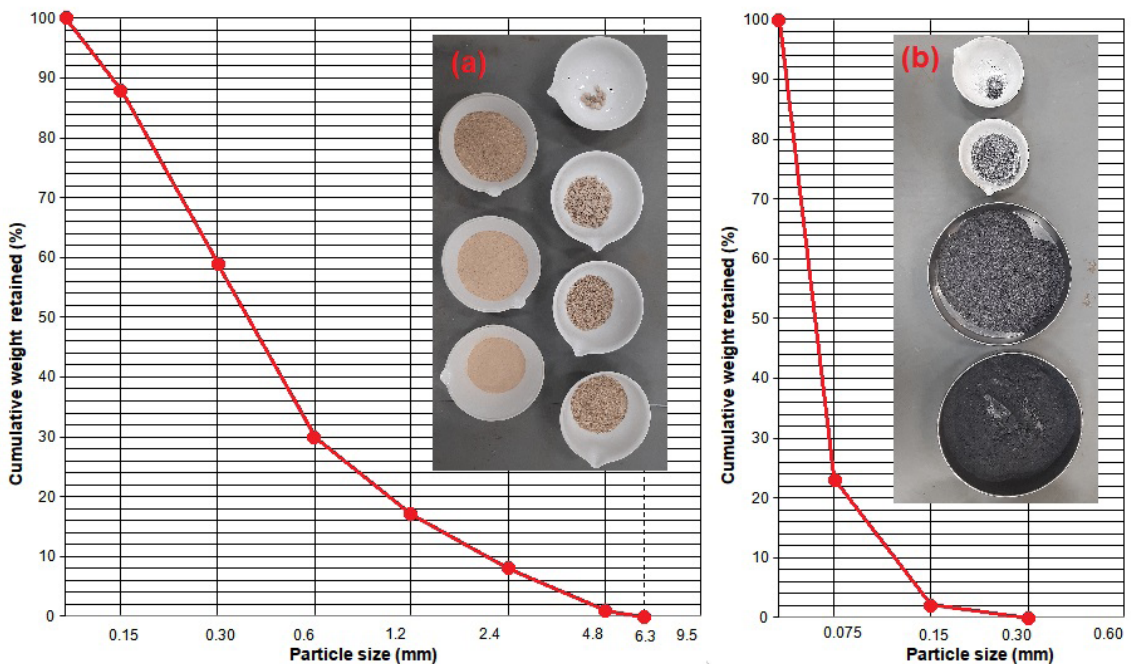


Figure 4. The granulometric curves of the sand (a) and graphite (b) samples.

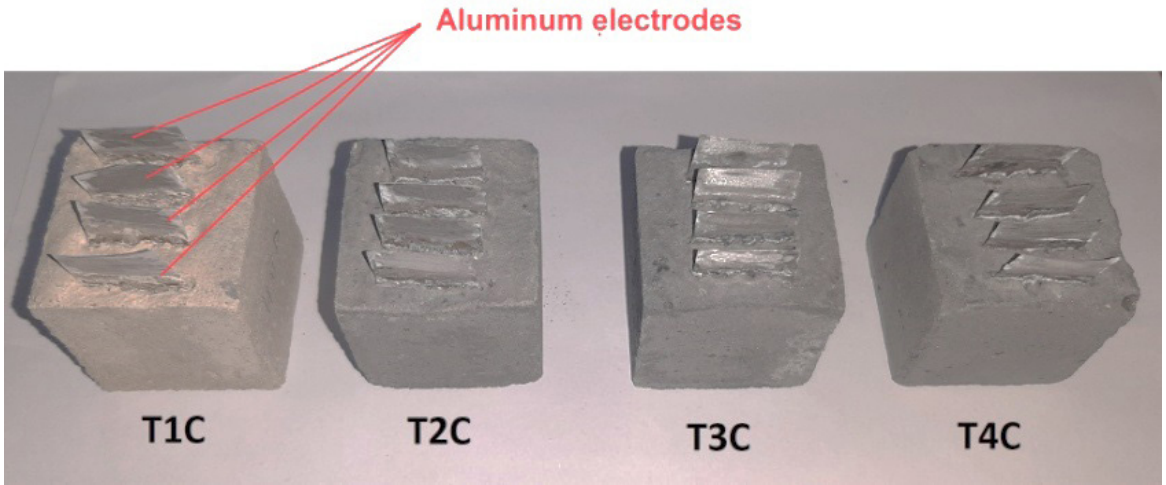


Figure 5. Cubic specimens with electrodes

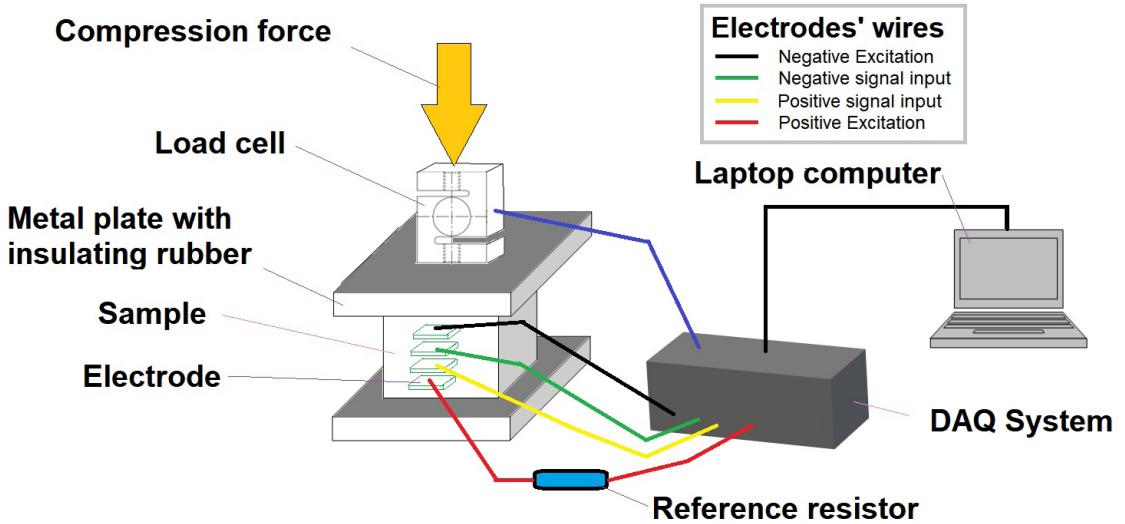


Figure 6. Data acquisition scheme of the experiment.

system (DAQ) model 8000-8-SM (Micro-Measurements), a load cell, and a laptop.

The electrical resistance was obtained from Ohm’s law<sup>41</sup> and, through the electrical circuit in Figure 7, it was possible to determine the electrical resistance ( $R_s$ ) of the composite by Equation 2 (adapted from<sup>53</sup>). A DAQ system was used to obtain the voltages in the sample ( $U_s$ ) and in the circuit supply ( $U_{in}$ ), with the use of a reference resistor ( $R_{ref}$ ) 1000  $\Omega$ <sup>34,54,55</sup>. The data from voltages in the sample ( $U_s$ ) corresponds to the wires green and yellow in Figure 6.

$$R_s = R_{ref} \frac{U_s}{U_{in} - U_s} \tag{2}$$

The electrical resistivity ( $\rho$ ) was calculated by Equation 3<sup>51,56</sup>, where the distance ( $L$ ) between the central electrodes and their contact area ( $A$ ) with the composite are known

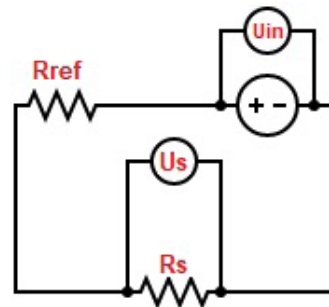


Figure 7. Electrical circuit for measuring electrical resistance (adapted from<sup>53</sup>).

values, while the fractional change in resistivity (FCR) was calculated using Equation 4<sup>2</sup>.

$$\rho = \frac{R_s * A}{L} \tag{3}$$

$$FCR \% = \frac{\Delta \rho}{\rho} * 100 \tag{4}$$

Among the ways indicated in the literature, the sensitivity<sup>22</sup> of the piezoresistive composite was determined from the fractional change of resistivity per unit stress ( $\sigma$ ), using Equation 5<sup>34,37-40</sup>.

$$S = \frac{FCR \%}{\sigma} \tag{5}$$

In other words, the sensitivity is the relationship between mechanical and electrical effects for the evaluation of piezoresistivity, when the resistivity can be affected by stress amplitude<sup>37-39</sup>.

Pearson's correlation ( $r$ ), coefficient of determination ( $R^2$ ) and other statistical parameters were determined using OriginLab Pro software, version 2021b.

### 3. Results and Discussion

According to literature<sup>33-36</sup> the applied force (compression) values and the fractional change in resistivity (FCR) obtained in the experiment are compared in the graphs of Figure 8, for each of the samples and repetitions, and a visual correlation analysis would be very subjective for qualifying the results, which is why a preliminary sensitivity analysis of the piezoresistive effect was performed.

The sensitivity analysis was made from the relationship between the peak values of the compression force and the FCR, using Equation 5, as shown in Table 1.

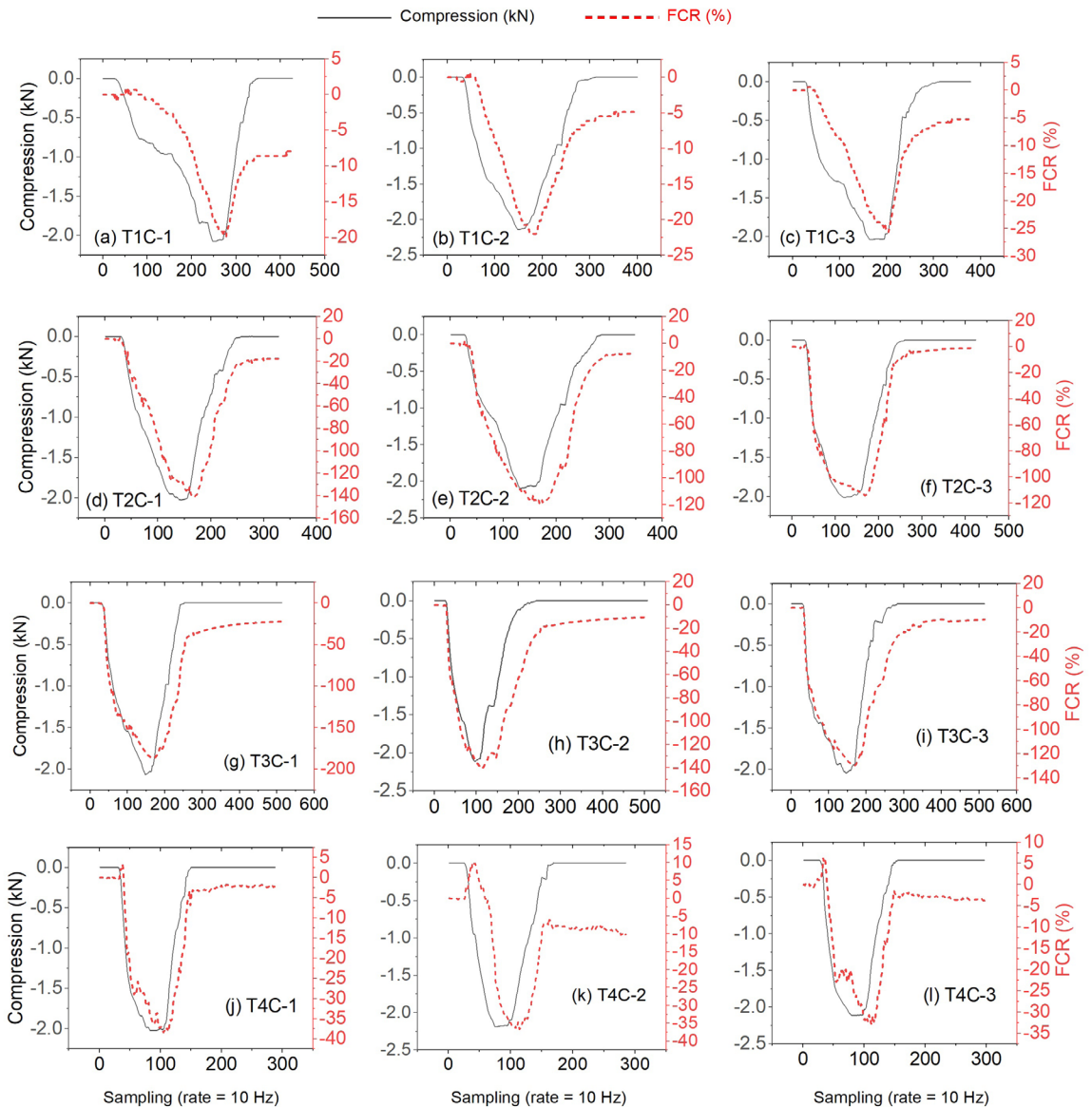


Figure 8. Compressive force values and the FCR in each mix and repetition test for T1C (a, b, c), T2C (d, e, f), T3C (g, h, i) and T4C (j, k, l).

Through the sensitivity relationship, it was possible to verify that the T2C and T3C samples had better results compared to the other samples. This is even clearer when presented graphically in Figure 9, which shows the mean values and their standard deviations (SD).

Even though the sensitivity relationship analysis shows a better response of the T2C and T3C samples, it also makes evident the accentuated variations between repetitions. This is especially true for the T3C sample, which has a high standard deviation compared to the other samples.

In a preliminary linearity analysis, the graphs of Figure 10 were plotted, which visually show better results for the T2C and T3C samples, but also possible to the subjectivity of their interpretation.

The Pearson's correlation values ( $r$ ), based on the data in the graphs in Figure 8, and the coefficients of determination ( $R^2$ ) based on the data in the graphs in Figure 10, are shown in the graph in Figure 11. Although both coefficients ( $r$  and  $R^2$ ) have been plotted on the same graph, the direct comparison between them cannot be adequate because the first expresses values from -1 to 1, and the second from 0 (zero) to 1.

The means and standard deviations of each coefficient ( $r$  and  $R^2$ ) for the samples tested are shown in the graphs in Figure 12, where again the best results for samples T2C and T3C are shown.

The  $R^2$  values obtained for the T2C and T3C samples are close to those found in the literature available<sup>46</sup>, while the low correlation of the T1C sample is justified by the

**Table 1.** Sensitivity of samples based on FCR/Stress relationship.

Sample	Repetition	Peak Value		Sensitivity (Equation 5)
		Stress* (MPa)	FCR (%)	
T1C	1st	-1.30	-19.86	15.33
	2nd	-1.33	-21.97	16.46
	3rd	-1.27	-25.62	20.12
T2C	1st	-1.27	-140.79	111.20
	2nd	-1.31	-118.99	90.84
	3rd	-1.26	-114.24	90.92
T3C	1st	-1.29	-186.47	144.53
	2nd	-1.32	-140.54	106.49
	3rd	-1.28	-129.67	101.56
T4C	1st	-1.26	-38.36	30.39
	2nd	-1.37	-36.65	26.81
	3rd	-1.32	-33.01	25.01

\*Compression

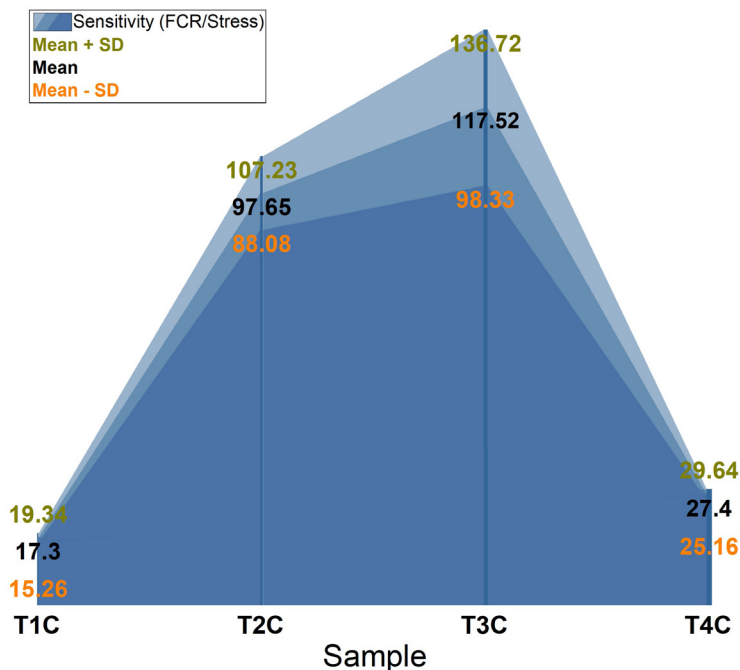


**Figure 9.** Mean sensitivity and standard deviations (SD) of samples.

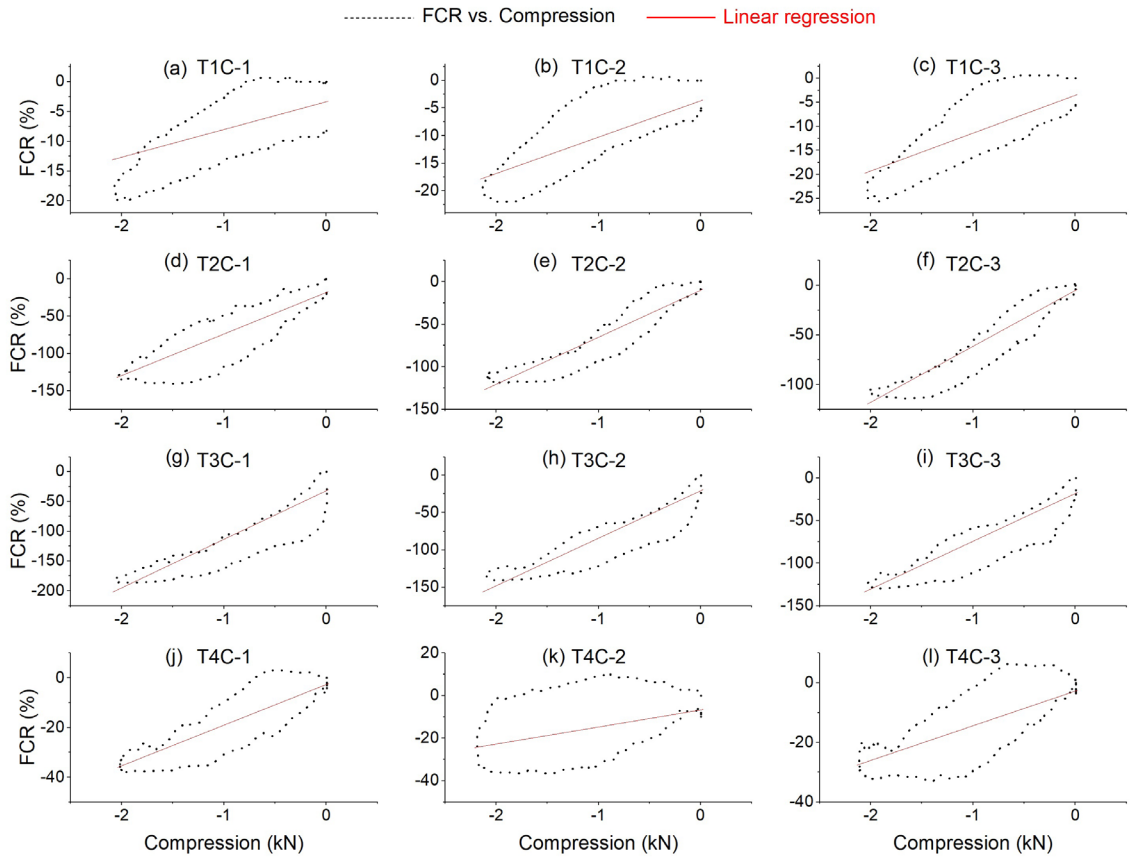


**Figure 10.** Graphical relationship between FCR and compression force, with linear regression (line in red) in each mix and repetition test for T1C (a, b, c), T2C (d, e, f), T3C (g, h, i) and T4C (j, k, l).

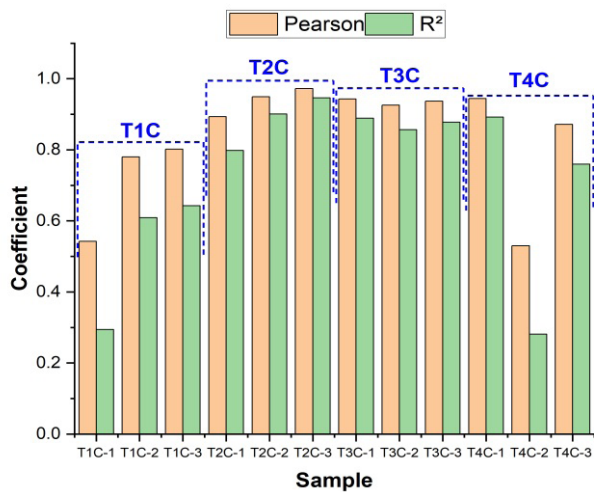


**Figure 11.** Pearson (r) and determination ( $R^2$ ) coefficients per sample.

absence of graphite and that of the T4C sample by the excess of graphite, which is also valid to justify the results obtained with the Pearson analysis.

For the final visualization of the results, each sample was ranked for each of the analyzes performed according to the table in Figure 13a, and each sample was spatialized

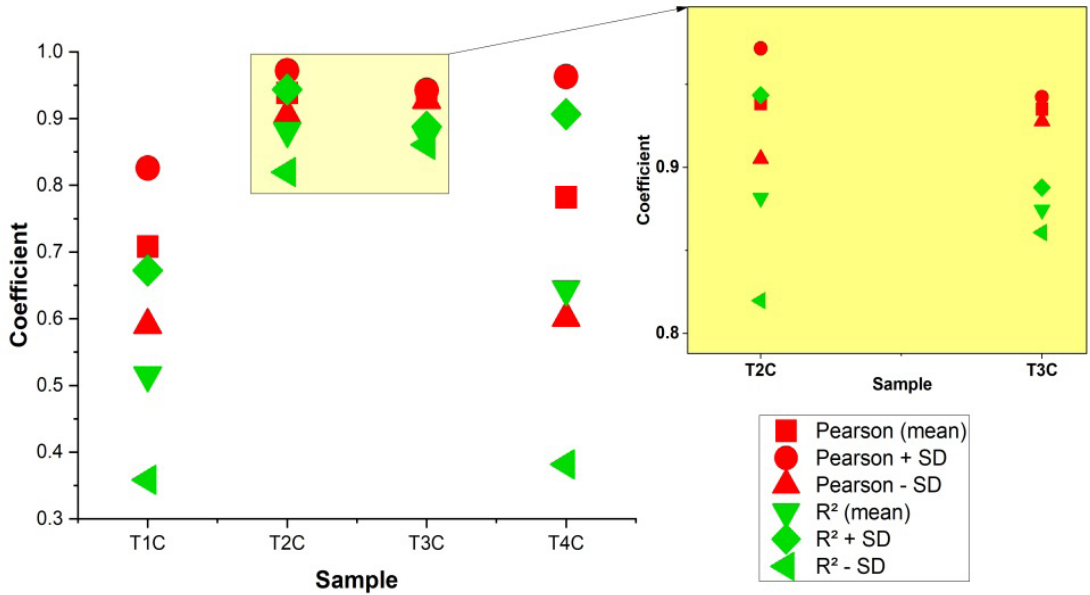
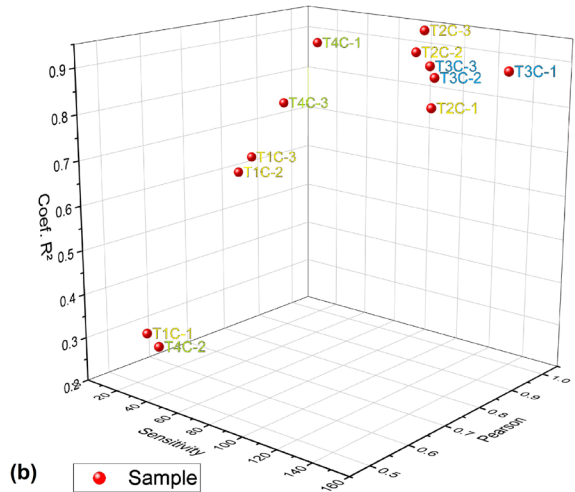


Figure 12. Mean and standard deviation per sample for each type of coefficient (r and R<sup>2</sup>).

Position	Sensitivity	Pearson	Coef. R <sup>2</sup>
1 <sup>o</sup>	T3C-1	T2C-3	T2C-3
2 <sup>o</sup>	T2C-1	T2C-2	T2C-2
3 <sup>o</sup>	T3C-2	T4C-1	T4C-1
4 <sup>o</sup>	T3C-3	T3C-1	T3C-1
5 <sup>o</sup>	T2C-3	T3C-3	T3C-3
6 <sup>o</sup>	T2C-2	T3C-2	T3C-2
7 <sup>o</sup>	T4C-1	T2C-1	T2C-1
8 <sup>o</sup>	T4C-2	T4C-3	T4C-3
9 <sup>o</sup>	T4C-3	T1C-3	T1C-3
10 <sup>o</sup>	T1C-3	T1C-2	T1C-2
11 <sup>o</sup>	T1C-2	T1C-1	T1C-1
12 <sup>o</sup>	T1C-1	T4C-2	T4C-2

(a)



(b)

Figure 13. Ranking table of the results per sample for each analysis parameter (a); spatialization of the results of each parameter in each sample (b).

according to the values of each parameter obtained, as shown in the graph in Figure 13b.

With the ranking shown (Figure 13a), the proportionality between the Pearson and determination coefficients becomes even more evident. Although they have different purposes, there is a quadratic relationship<sup>57,58</sup> between them. This relationship is shown in Figure 14, which exposes the analytical values of Pearson starting in 0.01 and moving forward in centesimal fractions to 1.00. Then, the quadratic value of Pearson that corresponds to R<sup>2</sup>, for each centesimal fraction, is plotted (Pearson *versus* R<sup>2</sup>). The experimental values of Pearson and R<sup>2</sup> of tested samples are plotted in the same graph (Figure 14), and are the same as the quadratic relationship analytical.

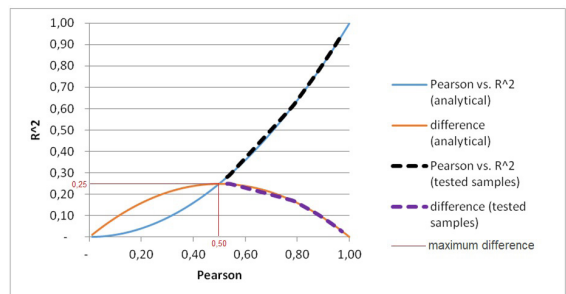


Figure 14. Analytical values (continuous line) and tested samples' values (dashed line) of Pearson *versus* R<sup>2</sup> and the difference between them; maximum difference (red line).

On the other hand, the graphic spatialization (Figure 13b) visually supported the best results obtained for T2C and T3C.

#### 4. Conclusions

Based on the results obtained, it can be considered that for the conditions and cases analyzed, the Pearson's coefficient has the potential to be used in the analysis of the correlation between changes in electrical resistivity and mechanical forces (or stress and strain) to verify the piezoresistive effect in self-sensing cementitious composites, although more studies are required to extrapolate these considerations to other cases and conditions.

We also saw that the higher the sensitivity, the standard deviation was higher too, which indicates that the repeatability was affected. But, in contrast to this, the correlation from Pearson ( $r$ ) and determination ( $R^2$ ) coefficients did not show that the repeatability was affected, because the higher the coefficients, the smaller the standard deviation.

It is also possible to pronounce that:

1. The evaluation of piezoresistive effect should not be limited only to graphical analysis of the values of electrical and mechanical parameters. Although it is important, this may lead to subjective or even mistaken interpretations, when not compared to numerical analysis;
2. The correlation analysis by Pearson must be limited to the linear behavior range of the study otherwise, other methods must be used;
3. The use of the Pearson correlation method should not exempt analysis by the coefficient of determination ( $R^2$ ) method, because they have different purposes. But, the first does not have the influence of a quadratic relationship in the results. The quadratic relationship makes the difference between the coefficients be minimum when approaching 0 (zero) or 1 (one) and maximum, when approaching 0.5 (half), as shown in Figure 14.

Determination of sensitivity, a relationship between FCR and stress, is also an important way of evaluating the self-sensing composite, although it has been observed (Figure 13) that few the sensitivity of the T4C-1 sample did not directly impact the bivariate correlation, as this sample obtained the 3rd position in the ranking of the Pearson and determination ( $R^2$ ) coefficients.

Lastly, both graphic and numerical evaluations (sensitivity and correlation coefficient) must be present in the analysis of the piezoresistive effect in self-sensing cementitious composites because, together, they allow a better interpretation of this effect.

#### 5. Acknowledgments

CAPES (Coordenação de Aperfeiçoamento de Pessoal de Nível Superior), Brasil - Financing Code 001; CNPq (Conselho Nacional de Desenvolvimento Científico e Tecnológico) - Prof. Luísa Andréia Gachet (310375/2020-7; 406234/2018-3) e Prof. Rosa Cristina Cecche Lintz (310376/2020-3).

#### 6. References

1. Sofi A, Regita JJ, Rane B, Lau HH. Structural health monitoring using wireless smart sensor network: an overview. *Mech Syst Signal Process.* 2022;163:108113.
2. Tian Z, Li Y, Zheng J, Wang S. A state-of-the-art on self-sensing concrete: materials, fabrication and properties. *Compos, Part B Eng.* 2019;177:107437.
3. Al-Bahrani M, Bouaissi A, Cree A. Mechanical and electrical behaviors of self-sensing nanocomposite-based MWCNTs material when subjected to twist shear load. *Mech Adv Mater Struct.* 2021;28(14):1488-97.
4. Liu Z, Zeng M, Wang H, Wang X, Li Y, Zeng C. Toward flexible piezoelectrets with high environmental stability: a hybrid approach. *es materials and manufacturing. ES Mater Manuf.* 2022;17:73-82.
5. Saxena P, Shukla P. A comprehensive review on fundamental properties and applications of poly(vinylidene fluoride) (PVDF). *Adv Compos Hybrid Mater.* 2021;4(1):8-26.
6. Wang H, Li Y, Wang X, Liu Z, Ahmed M, Zeng C. Preparation and characterization of piezoelectric foams based on cyclic olefin copolymer. *Eng Sci.* 2021;16:203-10.
7. Liu X, Wu S. Study on the graphite and carbon fiber modified asphalt concrete. *Constr Build Mater.* 2011;25(4):1807-11.
8. Ahmad M, Al-Dala'ien RNS, Beddu S, Itam ZB. Thermo-physical properties of graphite powder and polyethylene modified asphalt concrete. *Eng Sci.* 2022;17:121-32.
9. Chen J, Zhu Y, Guo Z, Nasibulin AG. Recent progress on thermo-electrical properties of conductive polymer composites and their application in temperature sensors. *Eng Sci.* 2020;12:13-22.
10. Scholle P, Sinapius M. A review on the usage of continuous carbon fibers for piezoresistive self strain sensing fiber reinforced plastics. *J Compos Sci.* 2021;5(4):96.
11. Chung DDL. A critical review of piezoresistivity and its application in electrical-resistance-based strain sensing. *J Mater Sci.* 2020;55(32):15367-96.
12. Han G, Su YF, Ma S, Nantung T, Lu N. In situ rheological properties monitoring of cementitious materials through the Piezoelectric-based Electromechanical Impedance (EMI) Approach. *Eng Sci.* 2021;16:259-68.
13. Su YF, Han G, Kong Z, Nantung T, Lu N. Embeddable piezoelectric sensors for strength gain monitoring of cementitious materials: the influence of coating materials. *Eng Sci.* 2020;11:66-75.
14. Dong W, Li W, Vessalas K, Wang K. Mechanical and conductive properties of smart cementitious composites with conductive rubber crumbs. *ES Mater Manuf.* 2020;7:51-63.
15. Chung DDL. Self-sensing concrete: from resistance-based sensing to capacitance-based sensing. *Int J Smart Nano Mater.* 2021;12(1):1-19.
16. Mishra S, Chaudhary P, Yadav BC, Umar A, Lohia P, Dwivedi DK. Fabrication and characterization of an ultrasensitive humidity sensor based on chalcogenide glassy alloy thin films. *Eng Sci.* 2021;15:138-47.
17. Rohilla D, Chaudhary S, Umar A. An overview of advanced nanomaterials for sensor applications. *Eng Sci.* 2021;16:47-70.
18. Huang K, Wu Y, Liu J, Chang G, Pan X, Weng X, et al. A double-layer carbon nanotubes/polyvinyl alcohol hydrogel with high stretchability and compressibility for human motion detection. *Eng Sci.* 2022;17:319-27.
19. Huang Y, Luo Y, Liu H, Lu X, Zhao J, Lei Y. A subcutaneously injected SERS nanosensor enabled long-term in vivo glucose tracking. *Eng Sci.* 2021;14:59-68.
20. Gijare M, Chaudhari S, Ekar S, Garje A. Reduced graphene oxide based electrochemical nonenzymatic human serum glucose sensor. *ES Mater Manuf.* 2021;14:110-9.
21. Fraç M, Pichór W. Piezoresistive properties of cement composites with expanded graphite. *Compos Commun.* 2020;19:99-102.

22. Wang L, Aslani F. Development of self-sensing cementitious composites incorporating CNF and hybrid CNF/CF. *Constr Build Mater.* 2021;273:121659.
23. Al-Dahawi A, Sarwary MH, Öztürk O, Yıldırım G, Akın A, Sahmaran M, et al. Electrical percolation threshold of cementitious composites possessing self-sensing functionality incorporating different carbon-based materials. *Smart Mater Struct.* 2016;25(10):105005.
24. Lee SY, Le HV, Kim DJ. Self-stress sensing smart concrete containing fine steel slag aggregates and steel fibers under high compressive stress. *Constr Build Mater.* 2019;220:149-60.
25. Vlachakis C, Perry M, Biondi L. Self-sensing alkali-activated materials: a review. *Minerals.* 2019;10(10):885.
26. Han J, Pan J, Cai J, Li X. A review on carbon-based self-sensing cementitious composites. *Constr Build Mater.* 2020;265:120764.
27. Baak M, Koopman R, Snoek H, Klous S. A new correlation coefficient between categorical, ordinal and interval variables with Pearson characteristics. *Comput Stat Data Anal.* 2020;152:107043.
28. Armstrong RA. Should Pearson's correlation coefficient be avoided? *Ophthalmic Physiol Opt.* 2019;39(5):316-27.
29. Bedeian AG, Sturman MC, Streiner DL. Decimal dust, significant digits, and the search for stars. *Organ Res Methods.* 2009;12(4):687-94.
30. Akoglu H. User's guide to correlation coefficients. *Turk J Emerg Med.* 2018;18(3):91-3.
31. D'Alessandro A, Tiecco M, Meoni A, Ubertini F. Improved strain sensing properties of cement-based sensors through enhanced carbon nanotube dispersion. *Cement Concr Compos.* 2021;115:103842.
32. Ding S, Wang YW, Ni YQ, Han B. Structural modal identification and health monitoring of building structures using self-sensing cementitious composites. *Smart Mater Struct.* 2020;29(5):055013.
33. Rovnanik P, Kusák I, Bayer P, Schmid P, Fiala L. Electrical and self-sensing properties of alkali-activated slag composite with graphite filler. *Materials.* 2019;12(10):1616.
34. Kim TU, Le HV, Park JW, Eock SK, Jang Y, Kim DJ. Development of a smart concrete block with an eccentric load sensing capacity. *Constr Build Mater.* 2021;306:124881.
35. Suchorzewski J, Prieto M, Mueller U. An experimental study of self-sensing concrete enhanced with multi-wall carbon nanotubes in wedge splitting test and DIC. *Constr Build Mater.* 2020;262:120871.
36. Ferdiansyah T, Turatsinze A, Balaýssac JP. Design and characterization of self-sensing steel fiber reinforced concrete. *MATEC Web Conf.* 2018;199:11008.
37. Dong W, Li W, Wang K, Luo Z, Sheng D. Self-sensing capabilities of cement-based sensor with layer-distributed conductive rubber fibres. *Sens Actuators A Phys.* 2020;301:111763.
38. Fraç M, Szudek W, Szoldra P, Pichór W. The applicability of shungite as an electrically conductive additive in cement composites. *J Build Eng.* 2022;45:103469.
39. Konkanov M, Salem T, Jiao P, Niyazbekova R, Lajnef N. Environment-friendly, self-sensing concrete blended with byproduct wastes. *Sensors.* 2020;20(7):1925.
40. Monteiro AO, Cachim PB, Costa PMFJ. Self-sensing piezoresistive cement composite loaded with carbon black particles. *Cement Concr Compos.* 2017;81:59-65.
41. Del Moral B, Baeza FJ, Navarro R, Galao O, Zornoza E, Vera J, et al. Temperature and humidity influence on the strain sensing performance of hybrid carbon nanotubes and graphite cement composites. *Constr Build Mater.* 2021;284:122786.
42. Luo T, Wang Q. Effects of graphite on electrically conductive cementitious composite properties: a review. *Materials.* 2021;14(17):4798.
43. Holle MJ, Misak HE, Malik RA, Alarifi IM, Asmatulu R. Structural analysis and wear behavior of different graphite-based brushes for aircraft starter generator application. *Adv Compos Hybrid Mater.* 2021;4(1):162-72.
44. Hu X, Wu H, Lu X, Liu S, Qu J. Improving thermal conductivity of ethylene propylene diene monomer/paraffin/expanded graphite shape-stabilized phase change materials with great thermal management potential via green steam explosion. *Adv Compos Hybrid Mater.* 2021;4(3):478-91.
45. Loamrat K, Sappakittipakorn M, Sukontasukkul P. Application of cement-based sensor on compressive strain monitoring in concrete members. *Adv Mat Res.* 2014;931-932:446-50.
46. Chen M, Gao P, Geng F, Zhang L, Liu H. Mechanical and smart properties of carbon fiber and graphite conductive concrete for internal damage monitoring of structure. *Constr Build Mater.* 2017;142:320-7.
47. Tao J, Wang X, Wang Z, Zeng Q. Graphene nanoplatelets as an effective additive to tune the microstructures and piezoresistive properties of cement-based composites. *Constr Build Mater.* 2019;209:665-78.
48. ABNT: Associação Brasileira de Normas Técnicas. ABNT NBR 16868-2: structural masonry - part 2: execution and site control. Rio de Janeiro: ABNT; 2020.
49. Papanikolaou I, Litina C, Zomorodian A, Al-Tabbaa A. Effect of natural graphite fineness on the performance and electrical conductivity of cement paste mixes for self-sensing structures. *Materials.* 2020;13(24):5833.
50. ABNT: Associação Brasileira de Normas Técnicas – ABNT. ABNT NBR 7211: aggregates for concrete: specification. Rio de Janeiro: ABNT; 2009.
51. Cordon HCF, Tadini FB, Akiyama GA, Andrade VO, Silva RC. Development of electrically conductive concrete. *Rev Cerâmica.* 2020;66(377):88-92.
52. Han BG, Han BZ, Ou JP. Experimental study on use of nickel powder-filled Portland cement-based composite for fabrication of piezoresistive sensors with high sensitivity. *Sens Actuators A Phys.* 2009;149(1):51-5.
53. Monteiro AO, Loredó A, Costa PMFJ, Oeser M, Cachim PB. A pressure-sensitive carbon black cement composite for traffic monitoring. *Constr Build Mater.* 2017;154:1079-86.
54. Lima GES, Nalon GH, Santos RF, Ribeiro JCL, Carvalho JMF, Pedroti LG, et al. Microstructural investigation of the effects of carbon black nanoparticles on hydration mechanisms, mechanical and piezoresistive properties of cement mortars. *Mater Res.* 2021;24(4):e20200539.
55. Nalon GH, Ribeiro JCL, Araújo END, Pedroti LG, Carvalho JMF, Santos RF, et al. Effects of different kinds of carbon black nanoparticles on the piezoresistive and mechanical properties of cement-based composites. *J Build Eng.* 2020;32:101724.
56. Birgin HB, D'Alessandro A, Laflamme S, Ubertini F. Smart graphite-cement composite for roadway-integrated weigh-in-motion sensing. *Sensors.* 2020;20(16):4518.
57. Realini TDA. Prospective, randomized, investigator-masked evaluation of the monocular trial in ocular hypertension or open-angle glaucoma. *Ophthalmology.* 2009;116(7):1237-42.
58. Martins M. Coeficiente de correlação amostral. *Rev Cienc Elem.* 2014;2(2):42.